JOINT CENTER FOR SATELLITE DATA ASSIMILATION

NO. 61, FALL 2018

JCSDA Quarterly

NOAA | NASA | US NAVY | US AIR FORCE

DOI: 10.25923/jw00-r987

NEWS IN THIS QUARTER

Data Assimilation in the Next-Generation Global Prediction System (NGGPS) Era: Initial Implementation of FV3-based Global Forecast System (GFS)

As part of the National Weather Service (NWS) Research to Operations (R2O) initiative, the evolution toward a Next Generation Global Prediction System (NGGPS)[1] was started in 2014. Initial efforts were focused on evaluating new atmospheric dynamic cores as potential candidates for use as the global numerical weather prediction model at the National Centers for Environmental Prediction (NCEP). The initial decision would lay the foundation for phasing out the current operational global spectral model, a variant of which has been utilized for global numerical weather prediction over the past 35+ years. Upon completion of the first two phases of the dynamic core inter-comparison effort, the Finite Volume on a Cubed Sphere (FV3) dynamic core from the National Oceanic and Atmospheric Administration (NOAA) Geophysical Fluid Dynamics Laboratory (GFDL) was selected for inclusion in NGGPS. The evolution toward NGGPS is now in phase 3, with emphasis on implementation of the FV3-based model into NOAA infrastructure and eventual operations. The FV3-based global model is slated to replace the operational Global Forecast System (GFS) global spectral model in January 2019, and will form the basis of NOAA's Unified Forecast System (UFS) to be utilized for prediction across all spatial and temporal scales.

[1] https://www.weather.gov/sti/stimodeling_nggps

(continued on page 2)

IN THIS ISSUE

After the selection of the FV3 dynamic core was made, the model was brought into the NOAA Environmental Modeling System (NEMS)[2] infrastructure. The NEMS architecture is based on the Earth System Modeling Framework (ESMF) and has been used for various applications at NCEP, such as the North American Model (NAM). As part of the infrastructure development, a "write-grid component" has been incorporated into the model to write out model history files on Gaussian latitude-longitude grids in NEMS-io format, which is the format that is currently being utilized by the operational GFS and will help facilitate the use of FV3-based output in various downstream models at NCEP.

The initial efforts on developing and testing the FV3-based GFS have leveraged the current operational GFS physical parameterizations. However, some changes have been incorporated into the initial version of the FV3-based GFS model, including:

- Replacement of the operational prognostic cloud scheme (Zhao and Carr, 1997) with a single moment, six-class cloud microphysics scheme from GFDL (Lin et al., 1983) type scheme)
- Stratospheric prognostic ozone (McCormack et al., 2006; NOAA Climate Program Office-funded project by Compo et al.)
- Middle atmospheric water vapor photochemistry (McCormack et al., 2008).

Data Assimilation for FV3-based GFS

The operational GFS and global data assimilation system (GDAS) utilize a GSI-based hybrid 4D Ensemble-Variational solver (4D EnVar, Kleist and Ide, 2015; Wang and Lei, 2014), which has been operational since 2016. The system has a deterministic component at T1534 (~13km) horizontal resolution and an 80 member ensemble run at T574 (~35km) horizontal resolution, all which utilize 64 hybrid sigma-pressure vertical layers and a model top of ~55km. The ensemble part of the system, designed to represent the analysis and background error covariances, utilizes a suite of "stochastic physics" to account for model error, including:

- Stochastic energy backscatter (SKEBS, Shutts, 2005)
- Stochastically perturbed physics tendencies (SPPT, Buizza et al., 1999)
- Stochastically perturbed boundary layer specific humidity (SHUM, Tompkins and Berner, 2008).

The ensemble is updated every cycle utilizing the ensemble square root filter (EnSRF) of Whitaker and Hamill (2002). The hybrid 4DEnVar deterministic analysis is performed on the ensemble grid (~35km analysis increment) and is used to replace the EnSRF analysis ensemble mean (e.g., so-called re-centering).

The data assimilation system for the FV3-based GFS has been designed to be as close as possible to the configuration summarized above. The following notable exceptions will be described in more detail:

- Analysis increment is produced on Gaussian lat-lon grid and interpolated to the FV3 native cubed-sphere grid

[2] http://www.emc.ncep.noaa.gov/index.php?branch=NEMS

(continued on page 3)

JOINT CENTER FOR SATELLITE DATA ASSIMILATION

5830 University Research Court
College Park, Maryland 20740

Website: www.jcsda.noaa.gov

EDITORIAL BOARD

Editor:
James G. Yoe

Assistant Editors:
Biljana Orescanin
Sandra L. Claar

Director:
Thomas Auligné

Chief Administrative Officer:
James G. Yoe

Support Staff:
Sandra Claar

- Use of stochastic physics is modified
- Horizontal resolution of ensemble and analysis increment is increased
- Total cloud condensate increment is no longer passed back to the model
- All-sky assimilation has been turned on for the Advanced Technology Microwave Sounder (ATMS) instrument

The GSI does not currently have the capability to operate on a non-rectangular grid, though native grid data assimilation will likely come as a result of the Joint Effort for Data assimilation Integration (JEDI) project in the future. The FV3 dynamic core utilizes a cubed-sphere grid, though with the advent of the write-grid component, forecasts are also available on the Gaussian lat-lon grids that the GSI and EnKF infrastructure can ingest with minimal changes required. This allows for the deterministic and ensemble analysis increments to be computed on the Gaussian grid, which are subsequently interpolated to the cubed-sphere grid within the model itself and added onto the native grid restart state.

The stochastic components that are used in the GFS spectral model have been modified and adapted for use within the NEMS-FV3 model. For the initial implementation, only SHUM and SPPT are targeted for use. While SKEBS is available as an option in the NEMS-FV3 model, technical work was ongoing at the time of freezing the system for parallel testing prior to implementation. To compensate, the amplitude parameters associated with SPPT and SHUM have been modified to be appropriate for use within the FV3-based GDAS.

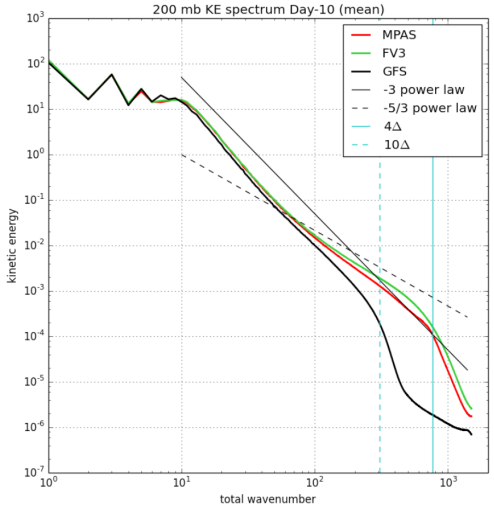

Figure 1. *10-day forecast 200 hPa kinetic energy (KE) spectra averaged over 74 cases. Reference power-law spectra corresponding to powers of -3 and -5/3 are shown for reference, as well scales corresponding to 4 and 10 times the nominal grid resolution (Figure 3.2 from Dynamic Core Evaluation Test Report for NOAA's NGGPS).*

One significant decision that was made early in the development and testing phase was to increase the spatial resolution of the ensemble to be exactly half of that the deterministic control. The prototype FV3-based GFS is configured to run at C768 resolution (~13 km) for the control, with an 80 member ensemble cycled at C384 (~26 km). This helps to reduce issues when interpolating between ensemble and control resolutions. The analysis increment is configured to be computed on a grid that also corresponds to the ensemble resolution. Furthermore, the "effective resolution" of the FV3 is higher than that of the global spectral model, even for comparable spatial discretization (Figure 1). The net result is a control forecast with higher "effective resolution," as well as ensemble forecasts (for the data assimilation) and analysis increments at significantly increased resolution.

In order to leverage the current data assimilation infrastructure, compromises had to be made in order to accommodate the new GFDL cloud microphysics scheme. The current operational GDAS/GFS system analyzes a total cloud condensate (a description of this within the context of

(continued on page 4)

all-sky assimilation can be found in Zhu et al., 2016). However, the introduction of the new microphysics scheme introduced an inconsistency between the cloud assimilation and the new background (and potential control variable) fields. As part of the initial effort, the cloud liquid water and cloud ice hydrometeors from the background are combined into a total cloud condensate in order to mimic current operations. Internal to the assimilation code, nothing is changed and a total cloud analysis increment is produced. However, this increment is never passed back to the model itself, but instead serves as a so-called "sink variable." In practice, the other control variables are being updated to be consistent with the total cloud increment through the multivariate correlations contained in the background error specification. Work is already underway to update all hydrometeors and will be part of a future upgrade.

While the initial all-sky radiance implementation in 2016 was limited to Advanced Microwave Sounding Unit (AMSU)-A radiances (Zhu et al., 2016), this capability has now been expanded to include ATMS radiances (Zhu et al., 2017). While many factors of the ATMS implementation are similar to that of AMSU-A, such as the observation error model, variational bias correction, and quality control, some adjustments had to be made specifically for ATMS radiances. Additional quality control was included due to the increased sensitivity to scattering for certain channels. The beam width for ATMS varies by channel, which poses an issue for the quality control and observation error assignment, thus spatial averaging was applied to enforce a common beam width. Special considerations were also made in the modeling of surface properties based on the FOV size and shape rather than an interpolation of the nearest four grid points as previously constructed.

Other aspects that have changed from the operational system are the recalibration of the background errors for near sea surface temperature (NSST), the omission of tropical cyclone relocation and the full field digital filter, and the inclusion of additional observations. The exclusion of tropical cyclone relocation comes about for both technical and scientific reasons. New observations include Geostationary Operational Environmental Satellite (GOES)-16 atmospheric motion vectors, NOAA-20 Cross-track Infrared Sounder (CrIS) and ATMS, and additional Infrared Atmospheric Sounding Interferometer (IASI) water vapor channels.

Testing and Evaluation of FV3-based GFS Forecasts

The transition to the FV3 dynamic core began in late 2016 with a free forecast capability through initialization from operational GDAS initial conditions. As components were developed, they were incorporated into the system piece by piece with a cycling capability becoming available in the summer of 2017. Testing for the data assimilation components was performed primarily within a lower resolution framework utilizing a horizontal resolution of C384 (~25 km) for the deterministic forecast and C192 (~50 km) for the analysis increment and ensemble forecasts. As components became mature and were sufficiently validated, they were incrementally added to a pseudo real-

(continued on page 5)

time parallel run at the target operational resolution.

The official field evaluation[3] of the implementation package began in late May 2018. In addition to the real-time system, three years of retrospective parallels (split into six streams) will be completed as part of the evaluation with numerous case studies being further examined. These experiments, case studies, and the field evaluations are expected to conclude in mid-September with a target implementation in January 2019.

Initial results from the retrospective parallels are encouraging. Figure 2 shows the 500 hPa geopotential height anomaly correlations (AC) for the first portion of two different streams out to day 7 for each hemisphere. The bottom panels show the percentage anomaly correlation change of each stream compared with the current operational system along with 95% confidence intervals. Both hemispheres exhibit statistically significant increases in skill through at least day four. The improvement in 500 hPa heights is further displayed in Figure 3, which contains the percentage change in root-mean-square error (RMSE) relative to the operational system. A statistically significant reduction in RMSE through day four is seen for both hemispheres and both retrospective streams (bottom left and bottom right panels). There is also a reduction in RMSE for the jet-level winds in the tropics and southern hemisphere for most lead times. The RMSE change for the jet-level winds in the northern hemisphere, as well as the lower tropospheric winds in the tropics, is generally neutral. Additional metrics, such as fits-to-observations

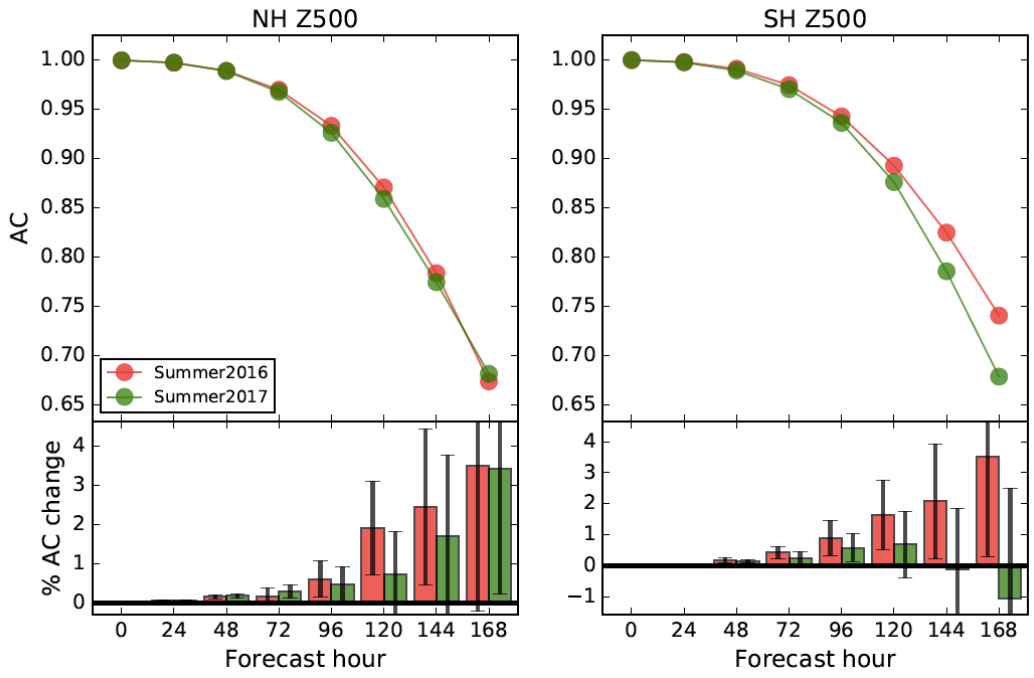

Figure 2. *Time averaged 500 hPa anomaly correlation (top portion of panels) for the Northern (left) and Southern (right) hemispheres as a function of forecast lead time for FV3-based GFS forecasts initialized at 00 UTC for the 2016 (red; 06 June 2016 through 20 July 2016) and 2017 (green; 10 June 2017 through 13 August 2017) boreal summer retrospective experiments. The bottom panel shows the difference of the experiments in terms of percent change relative to the operational GFS for the homogeneous set of cases for the 2016 (red) and 2017 (green) cases. The error bars represent 95% confidence threshold as derived from a student t-test.*

[3] *The official EMC evaluation page for the FV3-based GFS experiments is located here:* http://www.emc.ncep.noaa.gov/users/Alicia.Bentley/fv3gfs/

(continued on page 6)

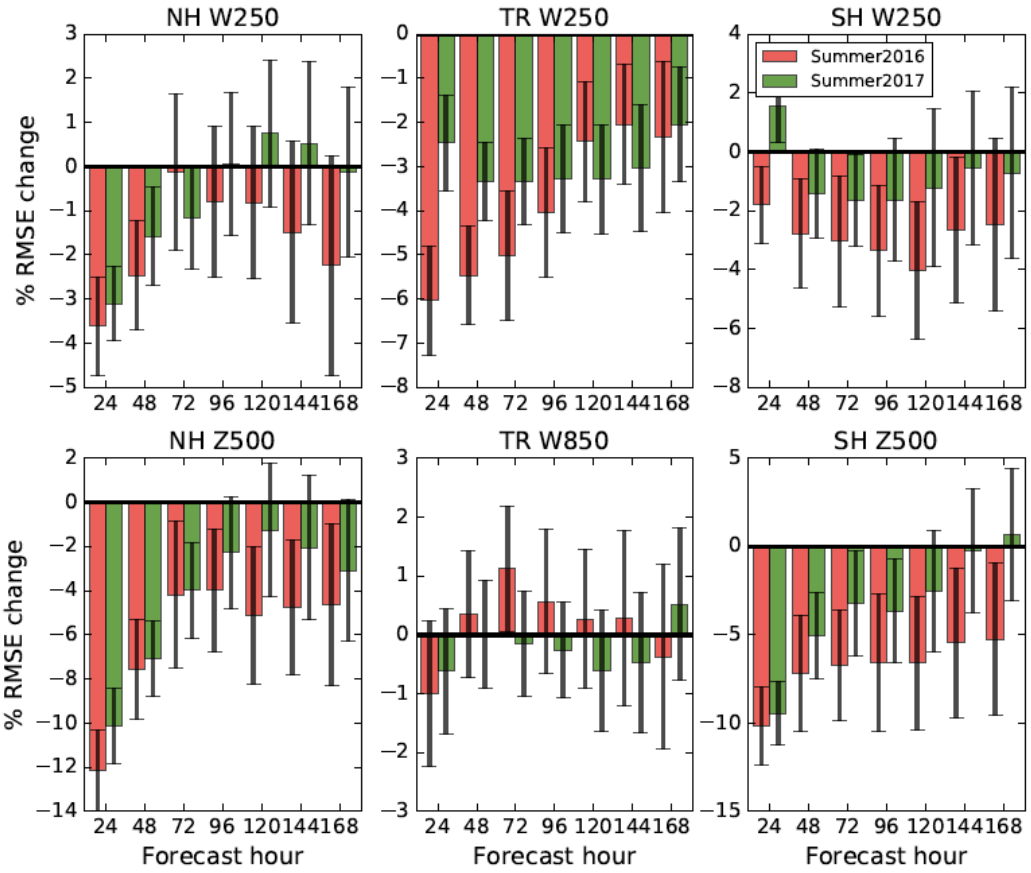

Figure 3. *Percent change in FV3-based GFS forecast root mean square error relative to the operational GFS (zero line) for various metrics (W-vector wind, Z-geopotential height), levels (mb), and regions (NH-northern hemisphere, TR-tropics, SH-southern hemisphere). Shown is the relative change as a function of forecast lead time for 00 UTC forecasts for the FV3-based GFS retrospective forecasts from the 2016 (red; 06 June 2016 through 20 July 2016) and 2017 (green; 10 June 2017 through 13 August 2017) boreal summer experiments. The error bars represent 95% confidence threshold as derived from a student t-test.*

and precipitation threat scores, show encouraging signs and improvements over the operational GFS (not shown).

The model evaluation group (MEG) has identified some individual cases demonstrating that the FV3-based GFS initial conditions appear more realistic than the operational GFS. One such example is from the genesis of eastern Pacific tropical storm Emelia (2018). Operational forecasters noted unrealistic multiple sea level pressure minima in the initial conditions from the operational GFS for two particular cycles when Emilia was still a tropical depression (Figure 4a and 4b). The corresponding initial conditions from the FV3-based GFS appear much more realistic, exhibiting a single, consolidated center (Figure 4c and 4d) more closely aligned with observations. While preliminary results from the full suite of retrospectives show improved tropical cyclone track forecasts from FV3-based GFS, it has been noticed that the intensity is generally found to be weaker than the operational GFS for most storms (not shown). This is currently being investigated further and will be part of the full scale evaluation.

Developments toward the second FV3-based GFS implementation are underway. With the initial upgrade focused on adapting existing infrastructure, the follow-on implementation aims to make several advances in both the model and data assimilation system. An increase in vertical resolution is being considered,

(continued on page 7)

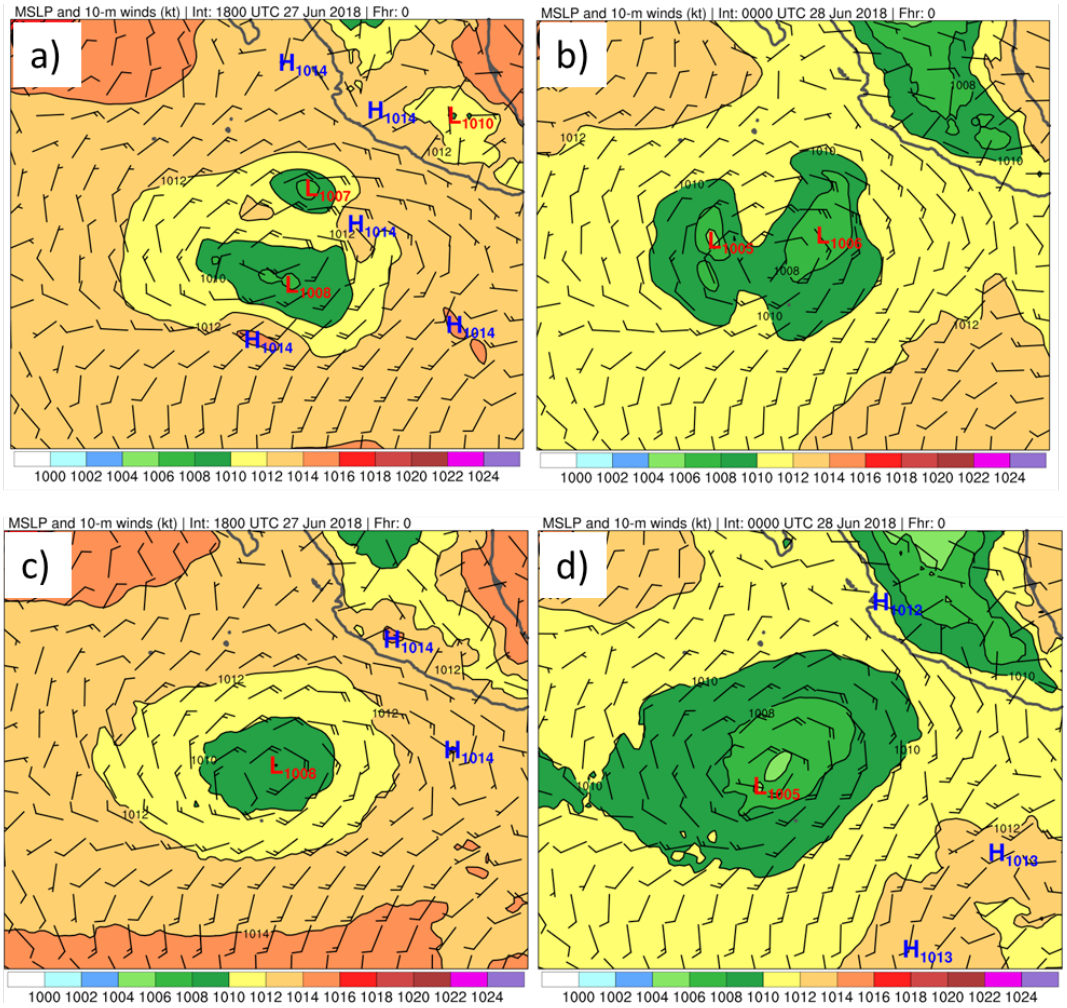

Figure 4. *Initial (00h) sea level pressure (color, 4 hPa contour) and 10m wind speed (barbs, knots) for eastern Pacific tropical depression (Emilia) from the operational GFS (top,a and b) and FV3-based GFS (bottom, c and d) valid at 1800 UTC 27 June 2018 (left, a and c) and 00 UTC 28 June 2018 (right, b and d).*

expanding from 64 to 127 vertical levels, and includes an increase of the model top from 55 to 80 km. This change requires the calculation of new static background error statistics and the evaluation of several existing components, such as the tangent linear normal mode constraint, stochastic physics, and channel selection for radiances. Other data assimilation components being considered include the 4D incremental analysis update, changing the EnKF solver to the Local Ensemble Transform Kalman Filter (LETKF), moving the EnKF update to the early cycle, scale dependent localization and weighting within the ensemble-variational solver, individual hydrometeor assimilation, and incorporation of correlated observation errors.

Authors

Daryl Kleist, NOAA/NWS/NCEP/EMC
daryl.kleist@noaa.gov
Rahul Mahajan, IMSG @ NOAA/NWS/NCEP/EMC
Catherine Thomas, IMSG @ NOAA/NWS/NCEP/EMC

(continued on page 8)

Acknowledgements
The work described in this article contains contributions from many people at NCEP/EMC and ESRL/PSD. We would like to specifically thank Fanglin Yang, Russ Treadon, Jun Wang, Jeff Whitaker, Phil Pegion, Yanqiu Zhu, and Andrew Collard. Thanks to Alicia Bentley and Geoff Manikin for discussion and figures related to tropical cyclone initialization.

References

Buizza, R., M. Miller, and T. N. Palmer, 1999: Stochastic Representation of model uncertanties in the ECMWF Ensemble Prediction System. *Quart. J. Roy. Meteor. Soc.*, 125, 2887–2908. doi: 10.1002/qj.49712556006.

Kleist, D.T., and K. Ide, 2015: An OSSE-Based Evaluation of Hybrid Variational–Ensemble Data Assimilation for the NCEP GFS. Part II: 4DEnVar and Hybrid Variants. *Mon. Wea. Rev.*, 143, 452–470, doi: 10.1175/MWR-D-13-00350.1.

Lin, Y., R.D. Farley, and H.D. Orville, 1983: Bulk Parameterization of the Snow Field in a Cloud Model. *J. Climate Appl. Meteor.*, 22, 1065–1092, doi: 10.1175/1520-0450(1983)022<1065:BOTSF>2.0.CO;2.

McCormack, J. P., S. D. Eckermann, D. E. Siskind, and T.J McGee, 2006: CHEM2D-OPP: A new linearized gas-phase ozone photochemistry parameterization for high-altitude NWP and climate models. *Atmos. Chem. Phys.*, 6, 4943–4972, doi: 10.5194/acp-6-4943-2006.

McCormack, J. P., K. W. Hoppel, and D. E. Siskind, 2008: Parameterization of middle atmospheric water vapor photochemistry for high-altitude NWP and data assimilation. *Atmos. Chem. Phys.*, 8, 7519–7532, doi: 10.5194/acp-8-7519-2008.

Shutts, G., 2005: A kinetic energy backscatter algorithm for use in ensemble prediction systems. *Quart. J. Roy. Meteor. Soc.* 131, 3079-3102, doi: 10.1256/qj.04.106.

Tompkins, A. M., and J. Berner, 2008: A stochastic convective approach to account for model uncertainty due to unresolved humidity variability. *J. Geophys. Res.*, 113, D18101, doi: 10.1029/2007JD009284.

Wang, X. and T. Lei, 2014: GSI-Based Four-Dimensional Ensemble–Variational (4DEnsVar) Data Assimilation: Formulation and Single-Resolution Experiments with Real Data for NCEP Global Forecast System. *Mon. Wea. Rev.*, 142, 3303–3325, doi: 10.1175/MWR-D-13-00303.1.

Whitaker, J.S. and T.M. Hamill, 2002: Ensemble Data Assimilation without Perturbed Observations. *Mon. Wea. Rev.*, 130, 1913–1924, doi: 10.1175/1520-0493(2002)130<1913:EDAWPO>2.0.CO;2.

Zhao, Q., and F.H. Carr, 1997: A Prognostic Cloud Scheme for Operational NWP Model. *Mon. Wea. Rev.*, 125, 1931–1953, doi: 10.1175/1520-0493(1997)125<1931:APCSFO>2.0.CO;2.

(continued on page 9)

Zhu, Y., E. Liu, R. Mahajan, C. Thomas, D. Groff, P. Van Delst, A. Collard, D. Kleist, R. Treadon, and J.C. Derber, 2016: All-Sky Microwave Radiance Assimilation in NCEP's GSI Analysis System. *Mon. Wea. Rev.*, 144, 4709–4735, doi: 10.1175/MWR-D-15-0445.1.

Zhu, Y., G. Gayno, P. v. Delst, E. Liu, R. Sun, J. Han, J. Derber, F. Yang, J. Purser, X. Su, J. Wang, and X. Li, 2017: Further developments in the all-sky microwave radiance assimilation and expansion to ATMS in the GSI at NCEP. The 21st International TOVS Study Conference Proceedings, Darmstadt, Germany, November 2017 (available online at http://cimss.ssec.wisc.edu/itwg/itsc/itsc21/proceedings/5p.02_zhu.pdf).

Efficient Data Selection Method for NWP Using Ensemble Forecast Sensitivity to Observations

The Ensemble Forecast Sensitivity to Observation (EFSO; Kalnay et al., 2012) technique provides efficient and economical impact evaluation for each observation by constructing a mapping between the future forecast error changes from data assimilation (DA) and the observation innovation. It belongs to a generic (FSO) family that also includes the Adjoint Forecast Sensitivity to Observations (AFSO); Langland and Baker, 2004) and the Hybrid Forecast Sensitivity to Observations (HFSO); Buehner et al., 2018). Under the context of the EFSO technique, a detrimental observation is identified as the observation with a positive EFSO value corresponding to forecast error increase when being assimilated and vice versa. There are mainly two applications of EFSO being proposed and examined: 1) Data monitoring and selection and 2) Proactive Quality Control (PQC).

The EFSO technique is computationally efficient and economical, allowing impact evaluation in near real-time with the operational numerical weather prediction (NWP) systems. In fact, several operational centers, including NASA/GMAO and NRL, are already releasing the online impact evaluation product. In addition to the monitoring tool, impact aggregation is another way to utilize the data, which allows evaluation of observational impact from various perspectives, such as radiance channels, data types, meteorological conditions, etc. A common practice is to aggregate the results with respect to the instruments, (e.g., Gelaro and Zhu, 2009; Ota et al., 2013; Hotta et al., 2017). The aggregated data can be utilized to identify a detrimental subset of the assimilated observations. This information can also be used for the improvement of model representation, data quality, and DA procedure in the long run; for the short-term, it can be used to improve existing data selection by blacklisting the observation subset that constantly degrades model forecasts. Lien et al. (2017)

(continued on page 10)

demonstrated using precipitation assimilation that EFSO provides more detail and accurate guidance on designing QC compared to simple trial and error.

To demonstrate the benefit of this application, we perform EFSO computation using a low-resolution GFS model coupled with LETKF/3D-Var Hybrid GSI (v2012) DA scheme (see Hotta et al. (2017) for the system configuration in detail). The experimental period covers from 00Z 10 Jan 2012 to 18Z 09 Feb 2012. The impact metric is the moist total energy error norm (MTE; Ehrendorfer et al., 1999) that includes and unifies the metric of the variables of interest in most meteorological applications: u- and v-component winds, temperature, surface pressure, and specific humidity.

As an example, we perform channel-wise impact evaluation for two hyperspectral instruments: Advanced Infrared Sounder (AIRS); Figure 1a) and Infrared Atmospheric Sounding Interferometer (IASI); Figure 1b). As expected, most of the assimilated channels are primarily beneficial. However, there are also some channels that contribute detrimental impact to the forecast. For IASI, those detrimental channels distributed within the wavelength range of 8–11 μm. Most AIRS channels in the same wavelength range are not assimilated, but many of the AIRS channels shorter than 8 μm are (but not for IASI). Only two channels around 4.58 μm show detrimental impact for AIRS. All these detrimental channels are largely sensitive to the conditions at the low-level or surface, where the brightness temperature of clouds is very close to that of the surface, which suggests that low clouds contamination may be a possible cause.

We then show the geographical source of these detrimental channel measurements in Figures

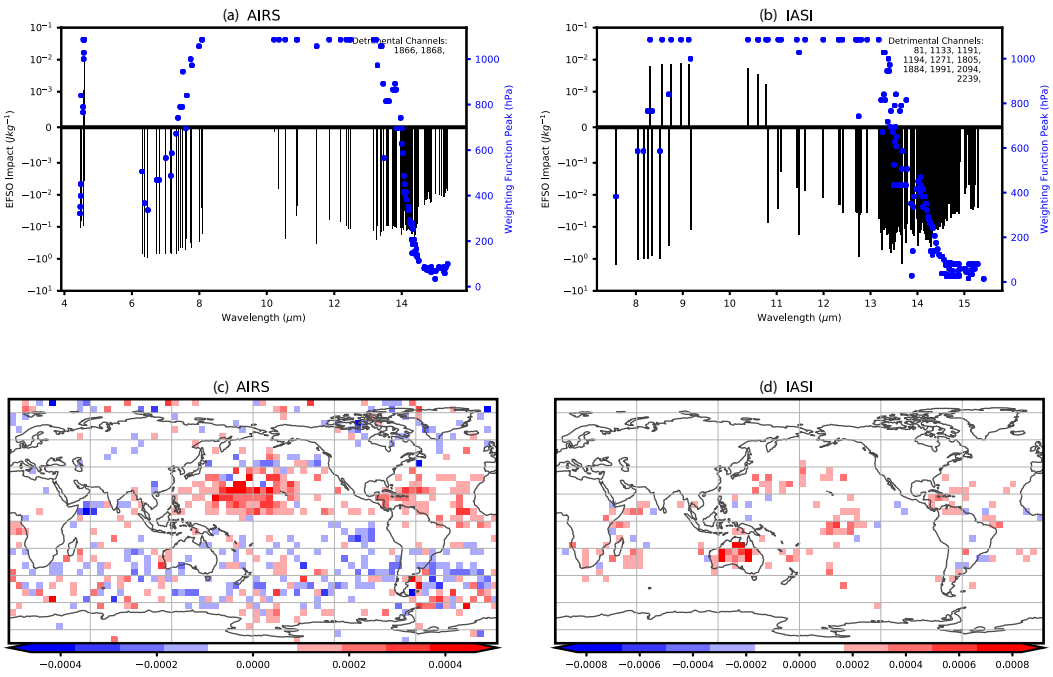

Figure 1: *(Top) Channel wise 6hr-EFSO impact evaluation of 2012 dataset for two hyperspectral instruments (AIRS and IASI). Each black line represents an assimilated channel and shows the EFSO impact [Jkg^{-1}]. The blue dots indicate the weighting function peak pressure level [hPa] of the channels. Net detrimental channels are listed on the upper-right corner. (Bottom) Geographic distribution of the impact [Jkg^{-1}] of the net detrimental channels.*

(continued on page 11)

1c and 1d. It reveals the specific regions where these detrimental measurements were taken. For AIRS, it is clear that the detrimental impact mainly comes from the northern tropical Pacific and Atlantic. Besides, these "detrimental" channels provide neutral to positive impact at higher latitudes, demonstrating again the detailed evaluation EFSO provides and the possibility of region-dependent data selection using EFSO. For IASI, the Australia continent and the oceans at low latitudes constitute the source of detrimental channels. The surface radiation representation of the Australia continent is notoriously difficult due to its special silica surface cover.

We also apply the same method for some multi-channel instruments, including GOES 13 and 15 sounders and High Resolution Infrared Radiation Sounder (HIRS). A common detrimental channel #13 (4.57 μm) for all three instruments and another channel #8 (11.03 μm) for GOES 13 are identified, and the detrimental measurements from both channels come from again the tropical oceans similar to those from hyperspectral instruments (not shown).

To verify the EFSO-identified detrimental channels, we perform a data-denial experiment that rejects the identified channels to see if the forecast is improved. The rejected channels and the corresponding wavelengths of each instrument are listed in Table 1. Recall the main detrimental impact is mostly from the Tropics, the relative error reduction for the tropical forecast is visualized in Figure 2. The forecasts for winds are generally improved throughout 6–7 day forecasts at different levels with maximum improvement centering around 700 hPa on day 2. The relative humidity shows similar improvements as the winds. The temperature improvement lasts for 3 days, shorter than for other variables. Overall, the forecasts reduce the errors about 1% for each variable.

This shows that the forecasts can still be improved as much as 1% by rejecting just 16 EFSO-identified detrimental channels out of hundreds. The significance of this denial experiment is a simple demonstration of the usefulness and accuracy of the EFSO impact evaluation.

For data selection processing, EFSO can be of greater use not by rejecting channels, but by adding back the beneficial channels that are currently not assimilated. Since EFSO depends on the quality of the analysis, we should not dump all the channels back into the system at once. Instead, the channels can be assimilated and

Table 1: *A list of rejected channels in the forecast verification experiment.*

Instrument	Rejected Channels	Wavelength [μm]
AIRS	1866, 1868	4.58, 4.58
GOES15 sounder	13	4.57
GOES13 sounder	8, 13	11.03, 4.57
HIRS	13	4.57
IASI	81, 1133, 1191, 1194, 1271, 1805, 1884, 1991, 2094, 2239	15.04, 10.78, 10.61, 10.60, 10.39, 9.12, 8.96, 8.75, 8.56, 8.30

(continued on page 12)

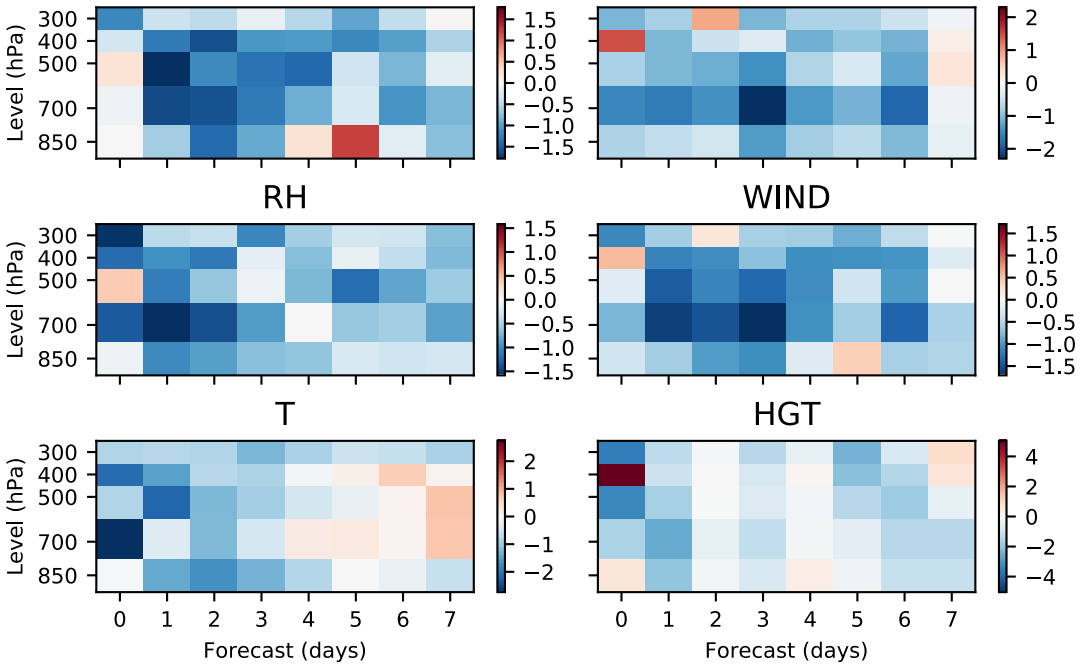

Figure 2: *Relative 7-day forecast error reduction [%] in the Tropics by rejecting detrimental channels identified by EFSO. Variables including u- and v-component wind, relative humidity, vector wind, temperature, and geopotential height for various pressure levels.*

evaluated with EFSO one small group at a time, and, in each iteration, we keep the channels with most substantial beneficial impact and compile a list of detrimental channels as in Rodgers (1996) but using EFSO instead of Degrees of Freedom of Signal (DFS). This way, we might be able to come up with a better channel selection than just using the DFS. Limited by the computational resources required to include the task in this study, we demonstrate that subtraction of data can already provide a considerable amount of improvement.

Proactive Quality Control (PQC), as opposed to the constant data selection with infrequent updates, rejects detrimental observations identified by immediate EFSO in each DA cycle that provides data QC in fully flow-dependent fashion. A non-cycling version of PQC was first pioneered in Hotta et al. (2017) to avoid "forecast skill dropout" issues for GFS (Kumar, 2009).

To show the benefit of cycling PQC, we used a faster and simpler GFS-LETKF system developed by Lien (2014). The NCEP GFS with lower-resolution (T62) is coupled with the generic LETKF core code developed and maintained by Takemasa Miyoshi (public Google Code platform: http://code.google.com/p/miyoshi/). The ensemble size is 32 with localization (Greybush et al., 2011) and inflation (Zhang et al., 2004; Miyoshi, 2011). Only the conventional observations provided in the prepBUFR dataset from NCEP are assimilated. Adjusting to the low resolution of our system, the observations are superobed/thinned to at most only one observation per model grid point for each data type and variable in one assimilation window, which reduces the data density to one-third of the original. We use the NCEP Climate Forecast System Reanalysis (CFSR); Saha et al., 2010) as truth to verify the PQC improvement on the analysis and the forecast. The experimental

(continued on page 13)

period covers one month from 00Z 01 Jan 2008 to 00Z 06 Feb 2008 using the first 5 days for DA spin-up.

PQC rejects detrimental observations based on EFSO in each cycle so that EFSO is computed in real-time when all required information is available, waiting for next analysis. After EFSO becomes ready, the analysis is repeated without the identified detrimental observations. In this experiment, we chose 6 hours as the forecast error verification lead-time for EFSO impact evaluation and reject approximately 10% of the overall most detrimental observations.

We first examine the monthly-averaged PQC corrections on the analysis from a map point of view. In Figure 3, we show the u-component wind, temperature, and humidity analysis corrections at 500 and 850 hPa. It is clear that the analysis error for u-component wind and temperature are reduced throughout the globe for the two pressure levels while the analysis error for specific humidity is reduced mainly in low latitudes, where the humidity is higher. A noticeable feature is that the u-component wind and temperature corrections are largest over the Southern Ocean.

The monthly mean of the relative improvement in GFS forecast (%) by cycling PQC is shown in Figure 4. It is clear that for all regions and the three listed key variables, the short-term forecast can be improved by as much as 10% or more for higher latitudes. Then, as the forecast advances through time, the improvement decreases, but the error reduction saturates at about 5% (not 0%) even after 5 days!

The cycling PQC improvement is further broken down into the immediate correction (non-cycling PQC) and the accumulated correction (improved background from PQC that takes place in the final analysis or GDAS). The immediate impact comes from the PQC update from the original analysis at current cycle, which is the same as the

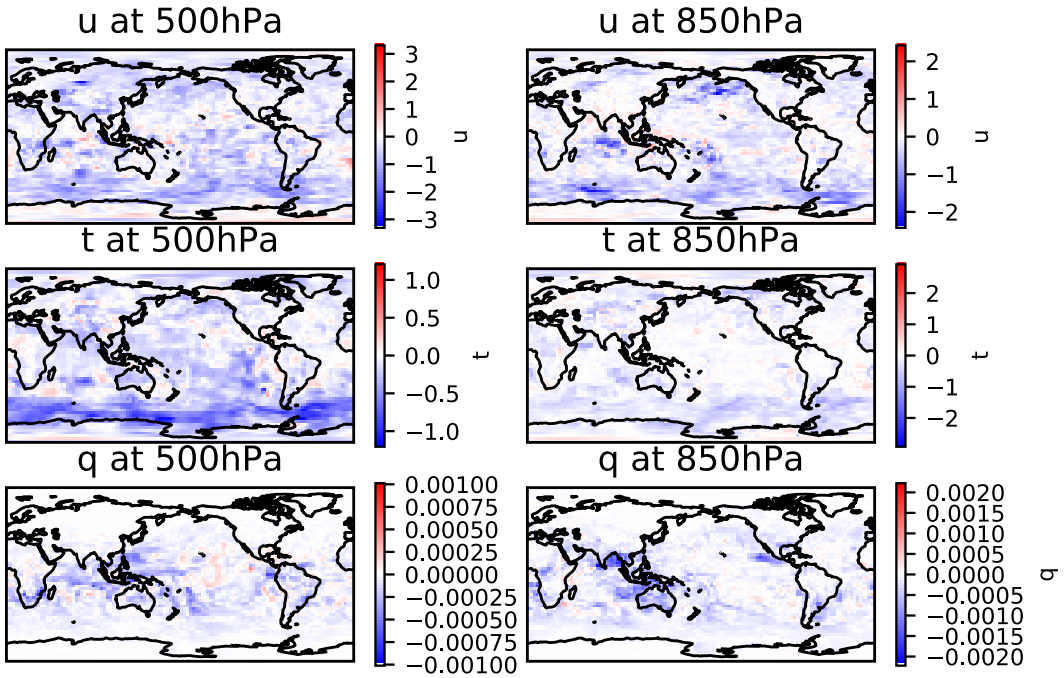

Figure 3: *Monthly mean analysis error (RMSE) reduction by PQC for u-component wind [u; ms^{-1}], temperature [t; K], and specific humidity [q; kgkg^{-1}] at 500 and 850 hPa.*

(continued on page 14)

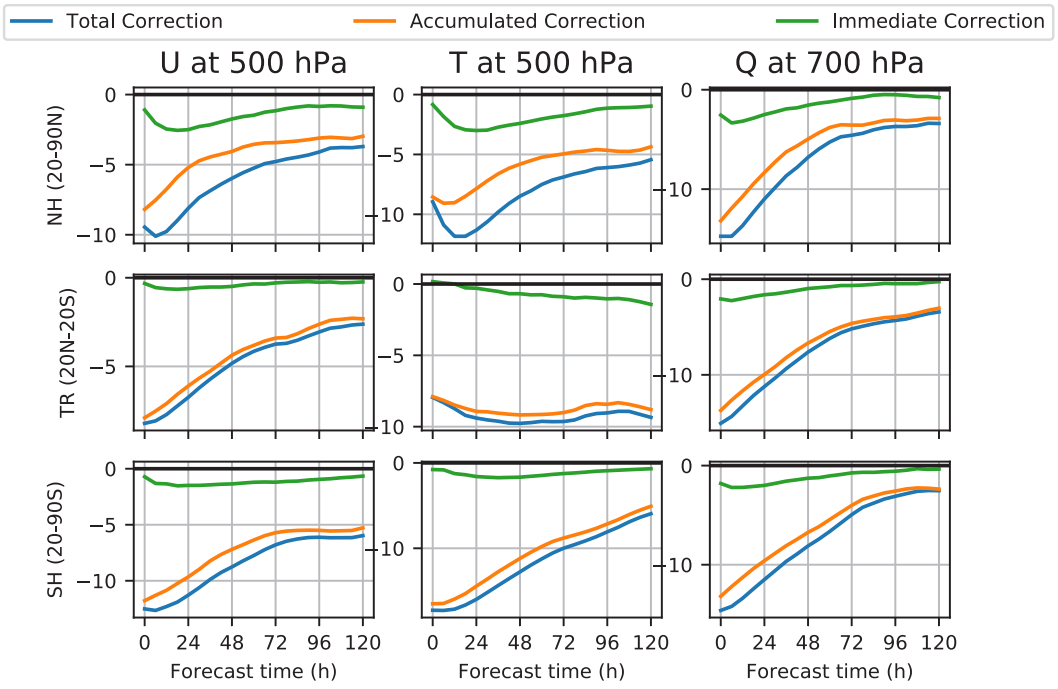

Figure 4: *Monthly mean relative forecast error (RMSE) reduction percentage initiated from cy-cling PQC analysis (full correction), original analysis in cycling PQC experiment (accumulated correction), and non-cycling PQC (immediate correction) in u-component wind at 500 hPa, tem-perature at 500 hPa, and specific humidity at 700 hPa for the Northern Hemisphere (20N-90N), the tropics(20N-20S), and the Southern Hemisphere(20S-90S) throughout 5 days.*

non-cycling PQC. The main benefit of cycling PQC is the accumulation of the improvements throughout the past cycles that the improved forecast initiated from the PQC-corrected final analysis, that then serves as a much more accurate background and further boosts the accuracy of the following analyses. We separate the accumulated correction from the full impact by verifying the forecasts initiated not from the PQC corrected analysis but from the original analysis before PQC (which is still improved by previous PQC corrections). As we can see, the primary advantage of cycling PQC comes from the accumulation of past improvements; whereas, the independent immediate improvement is only ~2%. It is also noticeable that the benefit from the accumulated impact has a more significant contribution to the full impact in the tropics and the Southern Hemisphere comparing to that in the Northern Hemisphere, indicating that the PQC improvement in the Northern Hemisphere has a shorter memory on the average.

The fact that the accumulation of past impacts contributes to a major portion of the full impact of cycling PQC has two important implications. One is that the PQC improvement has a long-term impact and remains in the system even after several cycles of DA. Secondly, this supports the feasibility of implementing PQC in operational NWP. The operational centers need to initiate the forecast as soon as the analysis is completed to deliver the forecast products on time, so we can only afford to perform PQC after the current forecast is out, meaning the immediate impact from PQC is not available in operations. Therefore, the significant portion of accumulated impact gives a very encouraging message that even without the immediate impact of the current PQC, the forecast improvement is still close to the full impact.

To conclude, we show promising results for both the initial attempt of EFSO-based channel selection that is verified with forecast

(continued on page 15)

improvement from the original selection and Proactive QC that improves the GFS analyses and forecasts in a rather simple experimental setup compared to the NCEP operational configuration. For future plans, we would like to explore adding beneficial channels based on EFSO from the large number of channels that are currently not assimilated. Furthermore, we will continue PQC exploration in DA system with close-to-operation configuration. It should be emphasized that the applications are not limited to EFSO but are applicable to all approaches of the generic FSO. By advancing in these two applications, the generic FSO technique has great potential to benefit both the observations and the model forecasts in NWP.

Authors

Tse-Chun Chen (University of Maryland) tcchen@umd.edu
Eugenia Kalnay (University of Maryland)

References

Buehner, M., P. Du, and J. Bédard, 2018: A New Approach for Estimating the Observation Impact in Ensemble–Variational Data Assimilation. Monthly Weather Review, 146 (2), 447–465, doi:10.1175/MWR-D-17-0252.1, URL http://journals.ametsoc.org/doi/10.1175/MWR-D-17-0252.1.

Ehrendorfer, M., R. M. Errico, and K. D. Raeder, 1999: Singular-Vector Perturbation Growth in a Primitive Equation Model with Moist Physics. Journal of the Atmospheric Sciences, 56 (11), 1627–1648, doi:10.1175/1520-0469(1999)056<1627:SVPGIA>2.0.CO; 2, URL http://journals.ametsoc.org/doi/abs/10.1175/1520-0469%281999%29056%3C1627%3ASVPGIA%3E2.0.CO%3B2.

Gelaro, R., and Y. Zhu, 2009: Examination of observation impacts derived from observing system experiments (OSEs) and adjoint models. Tellus, Series A: Dynamic Meteorology and Oceanog-raphy, 61 (2), 179–193, doi:10.1111/j.1600-0870.2008.00388.x.

Greybush, S. J., E. Kalnay, T. Miyoshi, K. Ide, and B. R. Hunt, 2011: Balance and Ensemble Kalman Filter Localization Techniques. Monthly Weather Review, 139 (2), 511–522, doi:10. 1175/2010MWR3328.1, URL http://journals.ametsoc.org/doi/abs/10.1175/2010MWR3328.1.

Hotta, D., T.-C. Chen, E. Kalnay, Y. Ota, and T. Miyoshi, 2017: Proactive QC: A Fully Flow-Dependent Quality Control Scheme Based on EFSO. Monthly Weather Review, (8), 3331–3354, doi:10.1175/MWR-D-16-0290.1, URL http://journals.ametsoc.org/doi/10.1175/MWR-D-16-0290.1.

Kalnay, E., Y. Ota, T. Miyoshi, and J. Liu, 2012: A simpler formulation of forecast sen-sitivity to observations: application to ensemble Kalman filters. Tellus A, 64, 1–9, doi:10. 3402/tellusa.v64i0.18462, URL http://www.tellusa.net/index.php/tellusa/article/view/18462/.

Kumar, K., 2009: Investigation of NCEP GFS Model forecast skill "dropout" characteristics using the EBI Index. URL https://ams.confex.com/ams/23WAF19NWP/techprogram/paper_154282.htm.

(continued on page 16)

Langland, R. H., and N. L. Baker, 2004: Estimation of observation impact using the NRL at-mospheric variational data assimilation adjoint system. Tellus A, 56 (3), 189–201, doi:10. 1111/j.1600-0870.2004.00056.x, URL http://onlinelibrary.wiley.com/doi/10.1111/j.1600-0870.2004.00056.x/fullhttp://tellusa.net/index.php/tellusa/article/view/14413.

Lien, G.-Y., 2014: Assimilation of Satellite Precipitation Analysis with the GFS-LETKF System. Ph.D. thesis, Ph. D. Prospectus, University of Maryland.

Lien, G.-Y., D. Hotta, E. Kalnay, T. Miyoshi, and T.-C. Chen, 2018: Accelerating assimilation development for new observing systems using EFSO. *Nonlinear Process. Geophys.*, **25**, 129–143, doi:10.5194/npg-25-129-2018. https://www.nonlin-processes-geophys.net/25/129/2018/.

Miyoshi, T., 2011: The Gaussian Approach to Adaptive Covariance Inflation and Its Implementa-tion with the Local Ensemble Transform Kalman Filter. Monthly Weather Review, 139, 1519– 1535, doi:10.1175/2010MWR3570.1.

Ota, Y., J. C. Derber, E. Kalnay, and T. Miyoshi, 2013: Ensemble-based observation impact estimates using the NCEP GFS. Tellus A, 65, 20 038, doi:10.3402/tellusa.v65i0.20038, URL http://www.tellusa.net/index.php/tellusa/article/view/20038/xml.

Rodgers, C. D., 1996: Information content and optimization of high-spectral-resolution mea-surements. Optical Spectroscopic Techniques and Instrumentation for Atmospheric and Space Research II, P. B. Hays, and J. Wang, Eds., Vol. 2830, 136, doi:10.1117/12.256110, URL http://proceedings.spiedigitallibrary.org/proceeding.aspx?doi=10.1117/12.256110.

Zhang, F., C. Snyder, J. Sun, F. Zhang, C. Snyder, and J. Sun, 2004: Impacts of Initial Esti-mate and Observation Availability on Convective-Scale Data Assimilation with an Ensemble Kalman Filter. Monthly Weather Review, 132(5), 1238–1253, doi:10.1175/1520-0493(2004) 132<1238:IOIEAO>2.0.CO;2, URL http://journals.ametsoc.org/doi/abs/10.1175/1520-0493%282004%29132%3C1238%3AIOIEAO%3E2.0.CO%3B2.

(continued on page 17)

Visualization, Evaluation, and Improvement of NWP-Based Cloud Analyses and Forecasts

Introduction

From its synoptic-scale origins, Numerical Weather Prediction (NWP) expanded to address both larger (coupled global climate system) and finer scale (nowcasting) forecasting. In particular, great strides have been made in the use of radar and other observations for the initialization of convective systems in their precipitating phase. This led to some initial successes in Warn-on-Forecasting (WOF) [*Stensrud et al., 2013*] of severe weather events and other nowcasting applications (WOF [*Bannister, 2007]*). While there is plenty of room for the extension of the predictability of severe events via the enhanced use of radar and other observations in the analysis of precipitating systems, this article explores another potentially significant, yet mostly untapped potential: the NWP analysis of clouds and aerosols. In this approach, rather than enhancing predictability of severe events by extending the span of useful forecasts for existing precipitating events, we extend it by stepping back in time and analyzing and forecasting cloud and aerosol conditions incipient to the emergence of the severe weather events themselves.

So far, the numerical analysis of clouds has remained as elusive as some clouds themselves. Progress in the areas of observations (e.g., visual imagery from new generation geostationary satellites and ground-based and airborne cameras), influence models (e.g., fast 3D visual radiative transfer models), data assimilation (e.g., 4dvar [*Bannister, 2007*]), and numerical modeling (e.g., advanced air chemistry and microphysics schemes) however, prime this area for rapid advances in the coming years. With careful design, the right tools, and proper funding, the next 5–10 years may see revolutionary advances in the realism of NWP-based aerosol and cloud analysis.

Current Image Observations

Sub-kilometer scale visible imagery is now becoming available with the latest generation of geostationary satellites updated as frequently as once per minute. This can supplement existing use of infrared (IR) satellite with radar and other data to provide a more complete description of the atmospheric state.

Expanding the range of vantage points to image the atmosphere, ground-based images from all-sky and other cameras are becoming more widely available. Commercial aircraft increasingly produce video imagery seen from the cockpit providing a horizontal viewing angle. We thus have a new collection of visible image data that can be harnessed for purposes of model evaluation and data assimilation.

(continued on page 18)

A Fast 3D Visual Radiative Transfer Model

Synthetic imagery simulated from model output is becoming more commonly used in some situations. This includes simulated IR satellite images and 2D visible light images from Community Radiative Transfer Model (CRTM). A 3D visible light imaging capability has been developed with systems such as MYSTIC (a rigorous Monte-Carlo method) [*Mayer, 2009*] and SHDOM [*Evans, 1998*], that uses spherical harmonics. Figure 1 illustrates various features of existing radiative transfer models, along with the new one described below called Simulated Weather Imagery (SWIm).

To help extend and make more operationally practical 3D visible light forward modeling, SWIm is being developed as a fast radiative transfer package. While special attention is being given to creating visually realistically images, where RGB image color hues and contrast are preserved in a side by side comparison between a computer monitor and the actual scene, the calculated spectral radiance and reflectance information can also be used for quantitative purposes. Consideration of various light sources (e.g., sun, moon, stars, city lights, airglow) and the spherical Earth allows SWIm to operate during daylight, twilight, and nighttime.

Figure 2 shows schematically how SWIm can convert model data into an image scene [*Albers, 2018*]. 3D model hydrometer (cloud liquid, cloud ice, rain, snow) and aerosol fields are converted to extinction coefficient and other optical properties. Radiative transfer equations are then applied to hydrometeor and aerosol optical thicknesses measured with forward and backward light rays to arrive at radiances based on single scattering. Figure 3 shows single scattering phase functions for four types of hydrometeors, illustrating how both

Figure 1. *Comparison of features among various radiative transfer models.*

Ray Tracing Techniques compared among RTMs

	SWIm	CRTM (current version)	RRTMG	SHDOM	Monte Carlo
3-D Radiation (including sideways between columns)	Y	N	N	Y	Y
Multiple Scattering	Approximate	Y	Y	Y	Y
Fast Running	Y	Y	Y	N	N
Ground- air- or space-based observer	All	Space	Space	All	All
Curved Earth Shadow / Twilight	Y	N	N		Y
Moon/Stars/City Lights	Y	N	N		
2-D (directional) images	Y	Y	TOA SW up (Isotropic)	Y	Y
Wavelengths	VIS	VIS + IR	VIS + IR		
Grid Resolutions	All	All	All	<=100m	All

(Klinger, Mayer et al., 2017)

(continued on page 19)

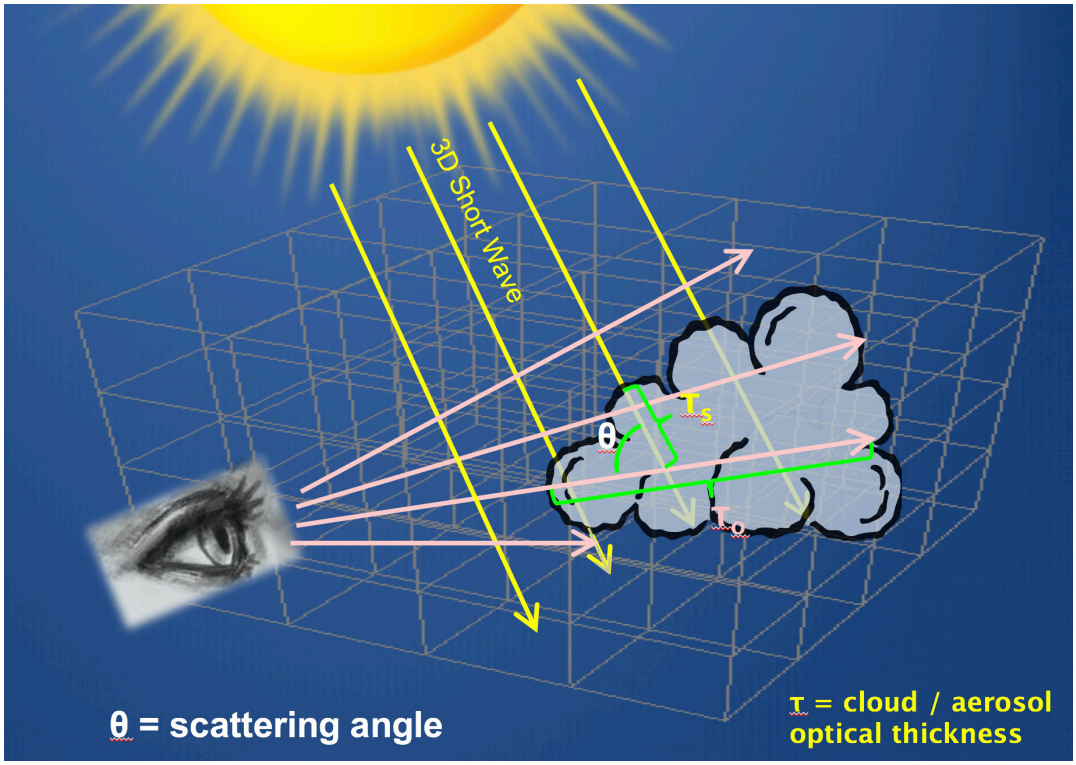

Figure 2. *Schematic diagram of the ray-tracing procedure showing forward light rays (yellow) coming from the light source. A second set of light rays (pink) are traced backward from the observer. The forward and backward optical thicknesses (τ_s and τ_o) are calculated along these lines of sight and used for subsequent calculations to estimate the radiance on an angular grid as seen by the observer.*

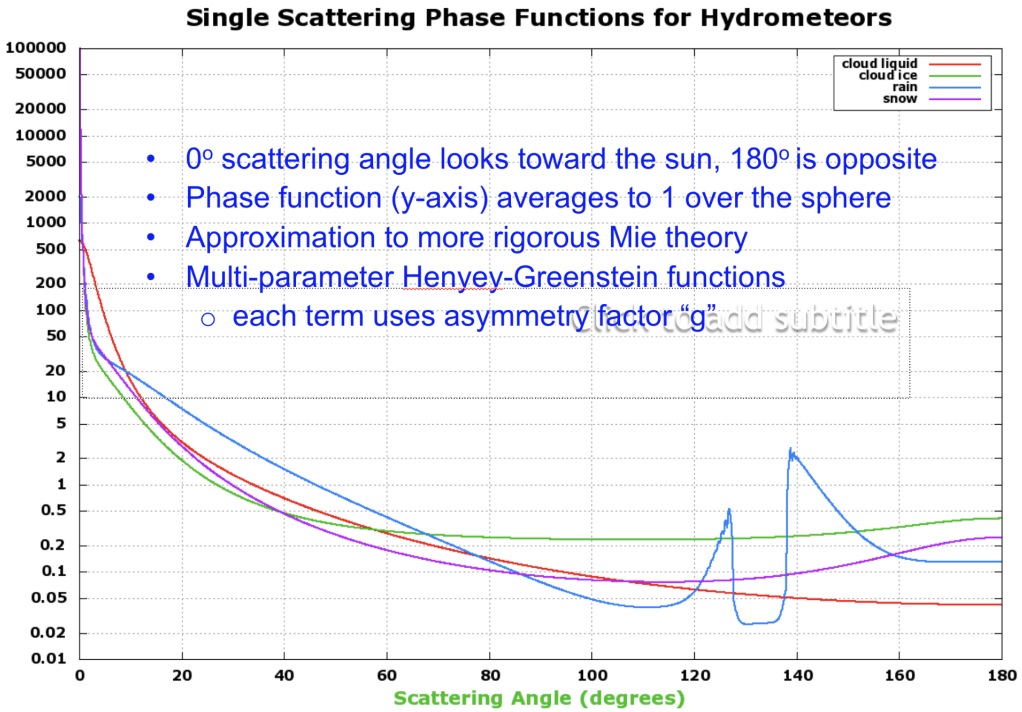

Figure 3. *Single scattering phase functions are shown for 4 types of hydrometeors: cloud liquid (red), cloud ice (green), rain (blue), and snow (purple).*

non-precipitating clouds and precipitation (e.g., rain shafts or virga) can be displayed. Multiple scattering is then addressed along each line of sight by parameterizing an equivalent or effective single-scattering phase function. The modified phase

(continued on page 20)

functions are flatter thus yielding a more uniform radiance distribution in the sky as clouds or aerosols become more optically thick.

This type of visualization can be used for forecast dissemination by weather offices and the media. It is possible to animate the forecast visual sky and landscape appearance for any desired location, allowing the viewer to intuitively perceptualize the weather. Web applications and flight simulators can also take advantage of this approach to feed NWP model data into sky visualizations. Figure 4 visualizes a forecast from NOAA's HRRR-Smoke system. We can vividly see the appearance from space of the wildfires in California during December, 2017.

Model Evaluation with SWIm

Cloud analyses running at resolutions of 500m showing current hydrometeor fields can be validated using SWIm by comparison to concurrent all-sky camera images. Figures 5 and 6 show several comparisons between a simulated all-sky images with an observed view at the same time. The simulated image (Figure 5 left) was derived from a LAPS

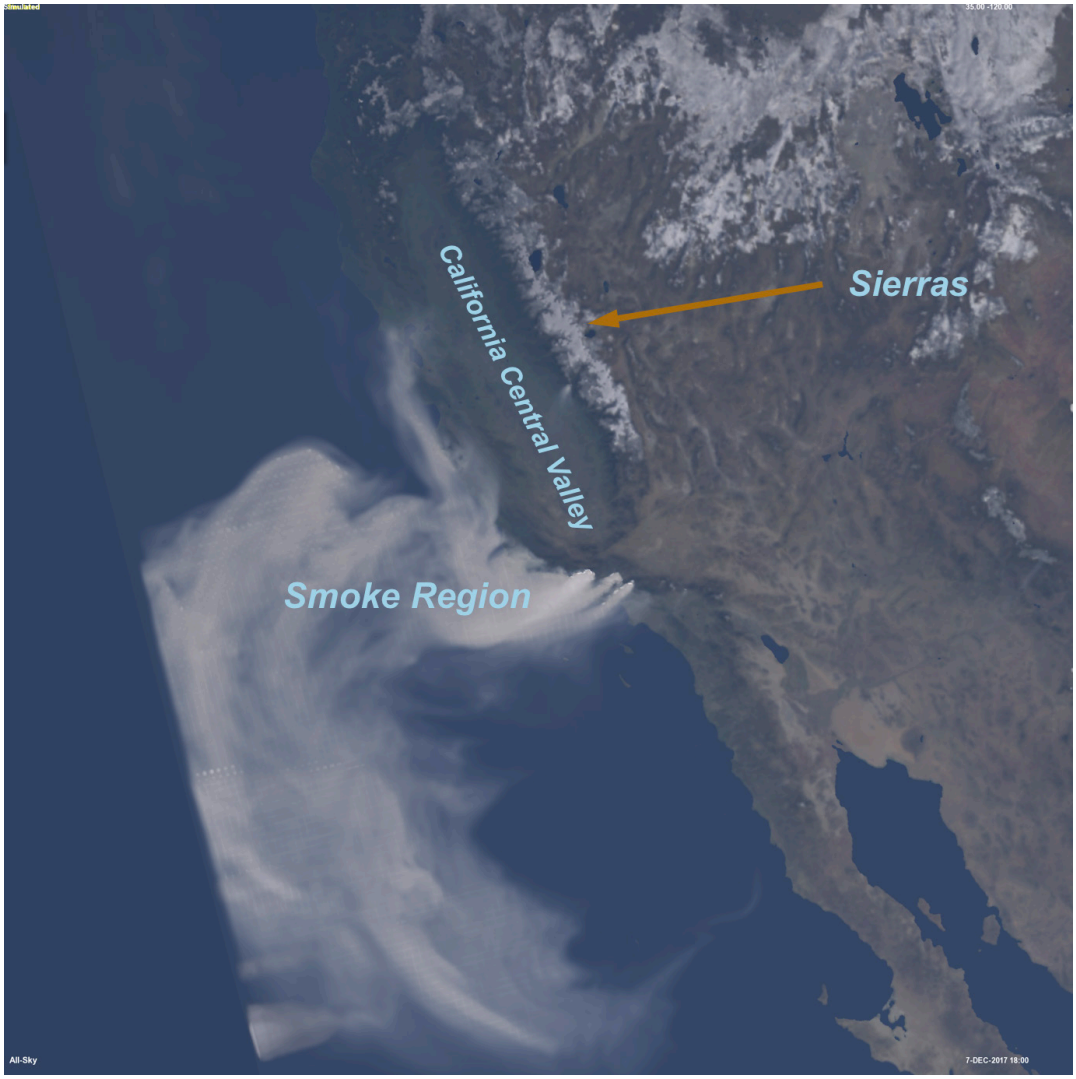

Figure 4. *Simulated image of a HRRR-Smoke forecast showing the smoke plume from California wildfires during December 2017. The view is zoomed in from a perspective point at 40000 km altitude.*

(continued on page 21)

cloud analysis running at 500m horizontal resolution on a 5-min update cycle. The 3D hydrometeor fields in the analysis are derived from satellite, radar, surface ceilometer observations, and model first guess fields. The camera image provides an independent validation of the analysis. In this case, the general outline of a thin high cloud deck is reasonably well placed. The simulated and observed cloud opacity (and optical thickness) is also reasonably well matched. This is evidenced by the intensity of the light scattering through the clouds relative to the surrounding blue sky, as well as the size and shape of the brighter aureole around the sun, if we account for the camera having a higher contrast presentation and more saturation of the image on the bright end. The saturated part of the solar aureole varies with optical thickness and reaches a maximum radius at $\tau \sim 3$. Four additional comparisons show the versatility of SWIm in various weather and lighting conditions (Figure 6). The upper right case shows clouds at night illuminated by both moonlight and city lights.

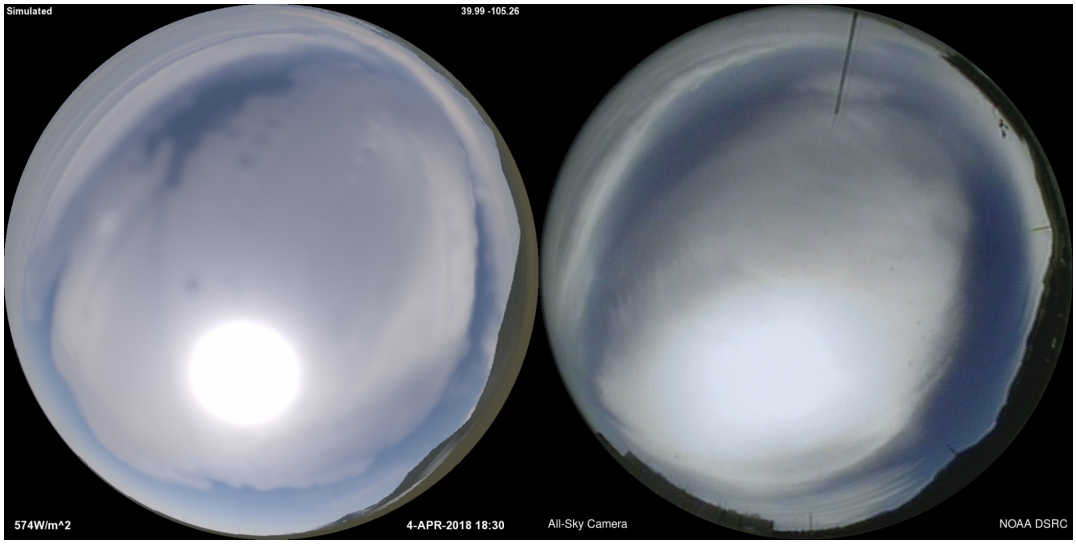

Figure 5. *Side-by-side montage of a SWIm image (left), and an all-sky camera image atop NOAA's Earth System Research Laboratory (right). North is up in these hemispheric views of the sky on a polar equidistant projection. Sunlight is scattering through a thin layer of clouds.*

Space-based Evaluation (e.g., DSCOVR/EPIC)

Figure 7 depicts a simulated view from a Global LAPS analysis (a) compared with a view from the EPIC instrument on NASA's DSCOVR satellite (b). Here we can holistically assess the analysis in terms of cloud placement and brightness, along with aerosols and land surface. Land surface multi-spectral albedo information is derived from NASA's Blue Marble Next Generation imagery. Details such as sun glint can be seen in the Pacific Ocean, opening the possibility of validating wind and ocean wave coupling. One can similarly display and assess analyses and forecasts from global models, such as FV3.

Objective Measures

SWIm can be used to generate cloud masks based on sky color and compare with corresponding cloud masks from camera images. These can be used in categorical skill score comparisons. Other measures use more continuous information from SWIm and the camera images including

(continued on page 22)

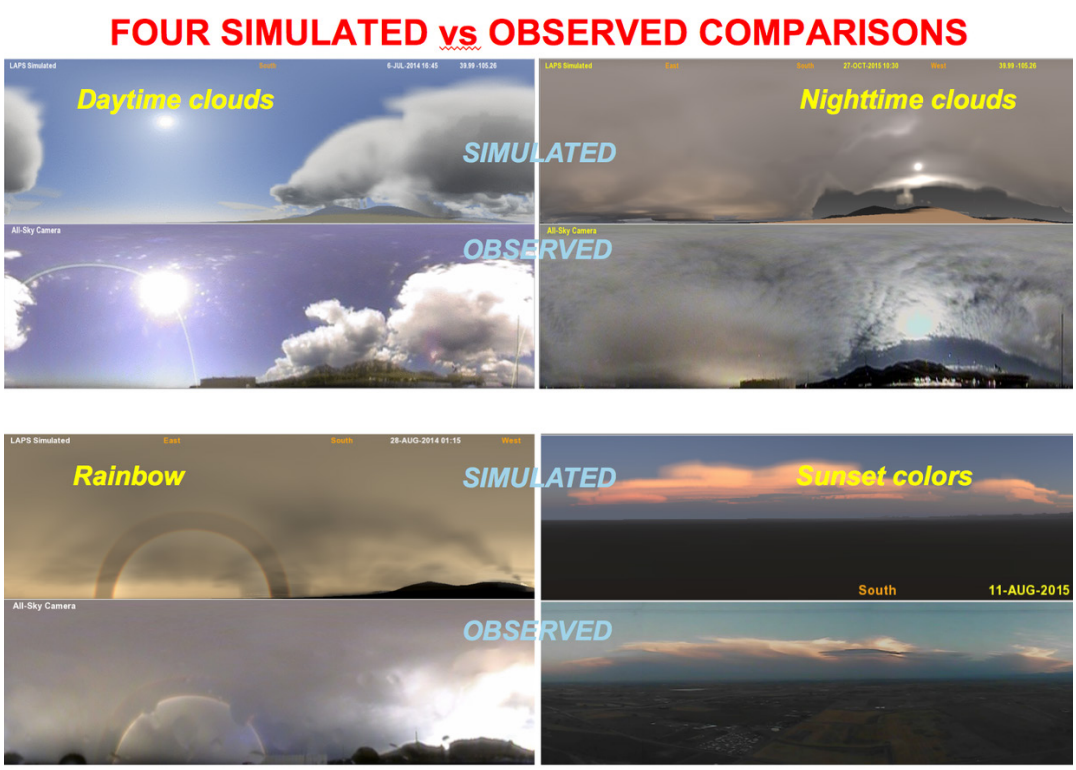

Figure 6. *Four simulated vs observed comparisons in a variety of weather and lighting conditions.*

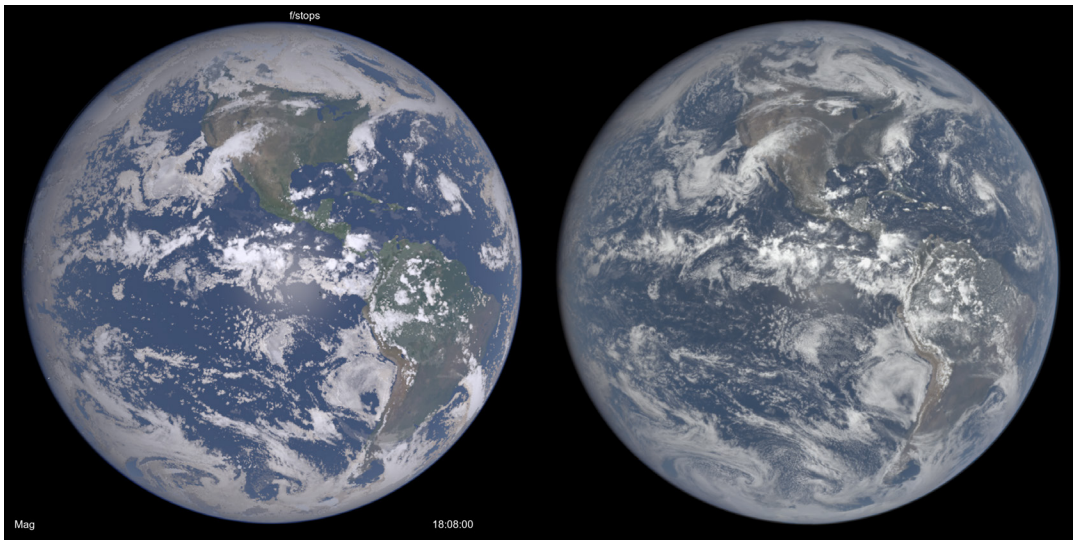

Figure 7. *Side-by-side montage (SWIm image on the left, DSCOVR:EPIC image on the right).*

correlation coefficient and RMS statistics. If the camera (or satellite) is calibrated in terms of radiance or reflectance, a more physically-based comparison can be performed.

(continued on page 23)

Vision for a Variational Multiscale Tomographic Cloud and Aerosol Analysis Module

With camera and satellite imagery available with 1-min frequency, a 4DVAR analysis can constrain the evolving model state to be consistent with observed cloud motions, allowing a more complete use of satellite data compared with 3DVAR. This has appealing advantages over satellite wind retrievals since separate assumptions about cloud height and layering are not needed.

The tomographic aspect of the analysis is two-fold. First, we are sensing the clouds from multiple viewing angles with an array of satellites and cameras. This helps constrain cloud geometry in much the same way as a Computed Tomography (CT) X-ray "diagnoses" shapes. Second, the intensity of scattered light in the high resolution visible wavelengths carries information about microphysical parameters throughout the volume of the clouds, since light can be scattered many times from various internal cloud locations.

The variational analysis operates by minimizing a cost function. This function has a series of forward operator terms where the model state is translated into observation space, and the differences are added together. Additional terms represent dynamical, physical, and statistical constraints.

SWIm can be used with camera images (and visible satellite images) as a forward operator to constrain model fields in a variational minimization. As ground-based camera networks and high-resolution geosynchronous satellite data become more available, one can consider a unified assimilation of these and other data sets in NWP models. 3D and 4DVAR have been proposed to utilize IR and visible satellite data [*Vukicevic et al., 2004*] and [*Polkinghorne and Vukicevic, 2011*]. We are experimenting with how camera images can be used as a penalty term in a variational cost function. One approach for determining the Pearson correlation coefficient r between observed and simulated all-sky images is shown on the same map projection. We are determining r for each of the R, G, B camera image channels and taking the mean value. This appears to do a good job of showing the degree of matching in the sky spectral radiance patterns.

To help work with more quantitative radiance values, two strategies are being considered. The first strategy would entail more precise calibration of camera exposure and contrast so images can be directly compared using an RMS statistic. A second strategy is being tested where we use the simulated image to estimate Global Horizontal Irradiance (GHI) and then comparing a GHI measurement made with a pyranometer collocated with the camera. The simulated GHI is estimated by examining a calculated field of spectral radiance at 550nm, then extrapolating this to the wavelength integrated radiance at each altitude and azimuth location. Correction factors based on atmospheric pressure and water vapor can be added. We can note that to a good approximation, colors in the sky, such as Rayleigh scattering, happen to have crossover points in their normalized spectrum to the solar spectrum that is close to the 550nm reference wavelength. The

(continued on page 24)

radiance values are then integrated over the hemisphere, normalizing by cos z to yield the irradiance.

Since SWIm operates in 3D and considers multiple scattering of visible light photons within clouds, it can help to perform what can be described as a tomographic cloud analysis. A preliminary version of this solving for a 3D cloud mask has been applied to a ground-based camera network as described in Viekherman et al., 2014. This has been expanded using airborne camera image radiances to perform a 3D cloud liquid water content analysis [*Levis, Schechner, Aides, 2015*] [*Levis, Schechner et al., 2015*] using a similar forward operator (SHDOM) in a variational solver using a recursive minimization. A corresponding aerosol Observation Simulation Experiment OSE analysis [*Aides et al., 2013*] was also performed with a ground-based camera network. Adjoint minimization can also be used [*Bannister, 2007*]. Multi-scale techniques can accelerate the minimization. Consideration of these studies suggests the possibility of bringing this all together to construct a tomographic 4DVAR cloud and aerosol analysis using multiple cameras and satellites (realizing their full spatial, temporal, and spectral resolution), radars and other data as in figure 8.

Summary

As exemplified by the unparalleled success of ECMWF, first 3D, then 4D variational data assimilation revolutionized synoptic-scale forecasting. With the advent of sub-kilometer scale imagery from a constellation of geostationary satellites and the proliferation of ground- and air-based photographic observations, we

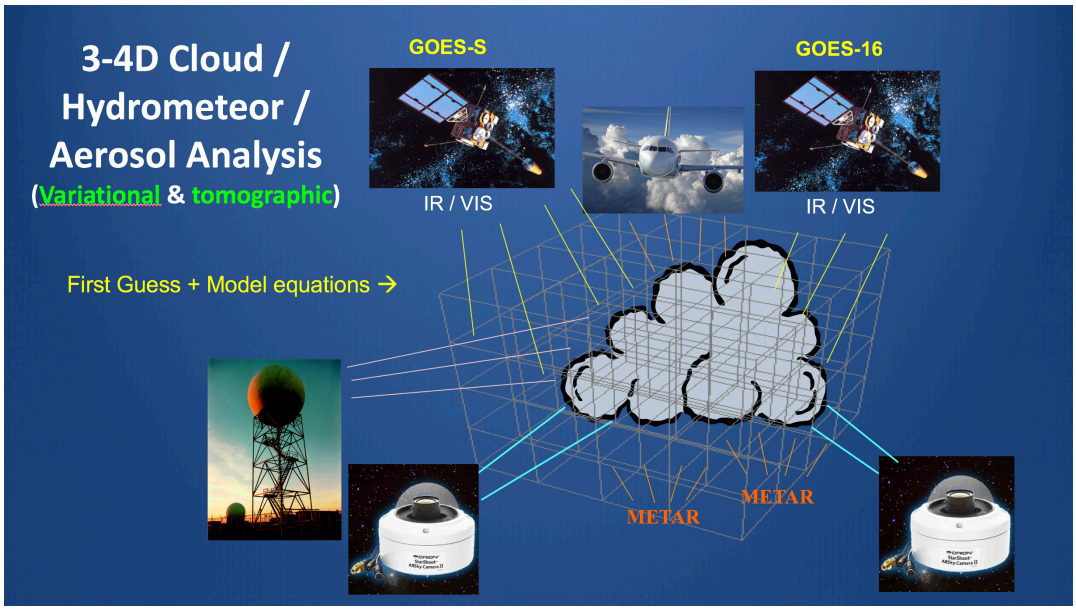

Figure 8. *Schematic diagram showing how multiple cameras and satellites can be combined with weather radar and other data in a 4D variational tomographic cloud analysis.*

(continued on page 25)

are at the cusp of another storm-scale forecasting revolution. Tomographic 3D or 4D variational assimilation of cloud-related data will take NWP-based nowcasting, including warn-on-forecast, to a new level. Realistic cloud analyses will allow us to backstep from the time of radar-observed convective initiation to the pre-convective environment, substantially increasing warning lead times for significant weather.

With the emergence of a fast 3D visible radiative transfer model (SWIm), the development of a 3/4D variational cloud and aerosol related data assimilation module can commence now, instead of waiting for future increases in computational power required by other forward imagery operators. After the incorporation of SWIm into CRTM, such a cloud/aerosol assimilation module can find its place in the JEDI repository, potentially benefiting the wide JCSDA user base from academic research to operations at multiple agencies.

Authors

Steve Albers - CIRA Steve.albers@noaa.gov
Zoltan Toth - NOAA

References

A. Aides, Y. Schechner et al.(2013), Multi sky-view 3D aerosol distribution recovery. *Optics express* **21** (22): 25820-33.

S. Albers et al. 1996: The Local Analysis and Prediction System (LAPS): Analyses of Clouds, Precipitation, and Temperature., *Weather and Forecasting*, **11**, 273-287.Bell, J. F. III, D. Savransky, and M. J. Wolff (2006), Chromaticity of the Martian sky as observed by the Mars Exploration Rover Pancam instruments, *J. Geophys. Res.*, **111**, E12S05, doi:10.1029/2006JE002687.

S. Albers. 2018: A fast 3-D Radiative Transfer Procedure at Visible Wavelengths for NWP Visualization and Forward Modeling, *Submitted to Atmospheric Measurement Technology*.

Bannister R. (2007), Elementary 4D-VAR, *DARC Technical Report No. 2. Data Assimilation Research Centre*, University of Reading, UK

Bell, J. F. III, D. Savransky, and M. J. Wolff (2006), Chromaticity of the Martian sky as observed by the Mars Exploration Rover Pancam instruments, J. Geophys. Res., **111**, E12S05, doi:10.1029/2006JE002687.

Bodhaine, B A et al. 1999: On Rayleigh Optical Depth Calculations. JTech **16**, 11, 1854-1861.

Doicu, A., D. Efremenko, T. Trautmann, 2013: A multi-dimensional vector spherical harmonics discrete ordinate method for atmospheric radiative transfer. *J. Quant. Spectrosc. Radiat. Transfer*, **118**, 121-131.

Evans, K. F., 1998: The spherical harmonic discrete ordinate method for three-dimensional atmospheric radiative transfer. *J. Atmos. Sci.*, **55**, 429-446.

D. Hestroffer, C. Magnan, Wavelength dependency of the Solar limb darkening, Astron. Astrophys. 333, 338–342 (1998)

H. Jiang et al. 2015: Real-Time Applications of the Variational Version of the Local Analysis and Prediction System (vLAPS). Bulletin of the American Meteorological Society **96** (12), 2045-2057

(continued on page 26)

Kleespies, T. J., P. van Delst, L. M. McMillin, and J. Derber (2004), Atmospheric transmittance of an absorbing gas. 6. An OPTRAN status report and introduction to the NESDIS/NCEP Community Radiative Transfer Model, Appl. Opt., 43, 3103 – 3109, doi:10.1364/AO.43.003103.

A. Levis, Y. Schechner, A. Aides, 2015:. Airborne Three-Dimensional Cloud Tomography. *2015 IEEE International Conference on Computer Vision (ICCV)* (2015): 3379-3387.

A. Levis, Y. Schechner, et al., 2015. An Efficient Approach for Optical Radiative Transfer Tomography using the Spherical Harmonics Discrete Ordinates Method. *arXiv*:1501.06093, 2015.

Louedec, K., Pierre Auger Collaboration & Losno, R. Atmospheric aerosols at the Pierre Auger Observatory and environmental implications, Eur. Phys. J. Plus (2012) 127: 97.

B. Mayer. Radiative transfer in the cloudy atmosphere. *European Physical Journal Conferences*., 1:75-99, 2009.

R. Polkinghorne and T. Vukicevic 2011: Data Assimilation of Cloud-Affected Radiances in a Cloud-Resolving Model. Monthly Weather Review. 139. 755-773. 10.1175/2010MWR3360.1.

T. Smith and J. Guild, The C.I.E. colorimetric standards and their use. 1931 Trans. Opt. Soc. 33 73

Stensrud, David et al. (2013). Progress and challenges with Warn-on-Forecast. Atmospheric Research. 123. 2-16. 10.1016/j.atmosres.2012.04.004. G. L. Stephens, 1978 Radiation Profiles in Extended Water Clouds. II: Parameterization Schemes *Journal of the Atmospheric Sciences* November 1978, **35**, (11)

Toth, Z., S. C. Albers, and Y. Xie, 2014: Multiscale Data Assimilation and Forecasting. *Bull. Amer. Meteor*. Soc.,**95** (2). ES30-ES33.

Dmitry Veikherman, Amit Aides, Yoav Y. Schechner and Aviad Levis, 2014: Clouds in The Cloud. Proc. ACCV.

T. Vukicevic et al. 2004: Mesoscale Cloud State Estimation from Visible and Infrared Satellite Radiances. Monthly Weather Review. 132. 10.1175/MWR2837.1.

J. Zhou et al. 2014: A Fast Inverse Algorithm Based on the Multigrid Technique for Cloud Tomography. Journal of Atmospheric and Oceanic Technology. **31**. 1653-1662. 10.1175/JTECH-D-13-00184.1.

(continued on page 27)

MEETING REPORT

Joint Workshop of the International Surface Working Group (ISWG) and Land Surface Analysis Satellite Application Facility (LSA-SAF)

On 26-28 June, 2018, at the Instituto Português do Mar e da Atmosfera (IPMA) in Lisbon, Portugal, the Joint Workshop of the 2nd International Surface Working Group (ISWG) and 8th Land Surface Analysis Satellite Application Facility (LSA-SAF) meetings was convened. This workshop saw over 15 countries represented by a dynamic, diverse, and engaging group with lively discussions.

The aim of the ISWG is to gather requirements specific to surface observations to enhance both our understanding and ability to monitor the components of the Earth system including land, vegetation, snow, ice, and coastal and open waters. The European Organization for the Exploitation of Meteorological Satellites (EUMETSAT) LSA-SAF aims to increase the benefits accrued from satellite data, specifically for terrestrial processes, land-atmosphere interactions and biospheric applications. One of the target applications of the LSA-SAF product is to assess and improve the quality of land surface models.

The meeting sought to combine and coordinate between the Earth System Modeling (ESM) and the data assimilation methodologies. The workshop opened with summaries from many numerical weather prediction (NWP) centers, such as Météo-France, ECMWF,

(continued on page 28)

Korea Meteorological Administration, and Deutscher Wetterdienst stating the current state of ESMs and their corresponding assimilation systems; as well an introductions to the land surface products distributed and maintained by the EUMETSAT LSA-SAF. An excellent brief by Dr. Sujay Kumar (NASA Hydrological Sciences Laboratory) highlighted some of the existing knowledge gaps, which remain in this difficult arena, particularly where remaining ESM systematic errors are not well treated in current data assimilation methods and require further fundamental research before they can be fully addressed.

The following presentations highlighted further the current state of the Earth surface products and assimilation methodologies where it is of note that there is beginning to be a focus on modifications of the number and density of the soil and snow levels in the ESMs; for example, Tomas Landelius of Swedish Meteorological and Hydrological Institute (SMHI) reported 14 soil layers and 12 snow layers in their current scheme. From the 1st ISWG, there was a call to examine the layering in the ESM models to accurately try to fit the observations, particularly those from L- and C-band, such as those from SMOS, SMAP (L-band) and AMSR-2 (C-band). Yohei Sawada from the Japanese Meteorological Agency presented a nice parameter sensitivity study of ESM parameters to the L- and C- band measurements also addressing another recommendation from the 1st ISWG. Both Drs. Sawada and Jean-Christophe Calvet (Météo-France) further showed that when trying to address the root zone soil moisture, the response of the vegetation has a clear signal, which can be utilized so that vegetation parameters in conjunction with surface soil moisture should be used to define the full soil state.

To aid in the development of accurate Earth System Models (ESMs), a critical parameter is still the surface temperature. An effort for a long term (since 1850) record of surface air temperature, the EUSTACE project (https://www.eustaceproject.eu/) was presented by Elizabeth Good of the Hadley Center of the UK Met Office. Further in for the more recent times, Frank-Michel Goettsche (Karlsruhe Institute of Technology) and Benjamin Bechtel (Uni Hamburg) showed methods of data reduction to provide parameters to create diurnal land surface temperature to which the ESMs can try to simulate realistic variability. While Carlos Jiménez of Estellus in France showed efforts to create a well-calibrated multi-decade land surface temperature from microwave to provide further consistent information for both the ESMs and many other applications.

The workshop plenary highlighted actions and recommendations for the community to take, which can further promote the uptake of observational data and Earth System Modeling (ESM). A short ESA CCI survey was circulated at the meeting aiming to capture the community needs regarding land surface temperature data. To participate in the survey, please contact Dr. Good at the Met Office (elizabeth.good@metoffice.gov.uk). Furthermore, a survey on L-band usage and plans from the SMOS-CESBIO is also being completed. The recommendations are largely ones that would lead to a roadmap for reduction in

(continued on page 29)

the bias or systematic errors the ESMs often show with respect to the observations. To further investigate these issues, a recommendation was set forth to cataloging important events for model study intercomparison, clearly defining the ESM and radiative transfer used for assimilation, continue parameter error-budget and sensitivity studies, and find the observations and other model parameters that correlate with the root zone soil moisture. Lastly, creation and maintenance of L- and C-band climatologies, along with those for Land Surface Temperature (LST), are critical to ensure the ESM is accurately depicting the diurnal and seasonal behavior.

The presentations and final plenary actions and recommendations are available on the workshop web page at: http://cimss.ssec.wisc.edu/iswg/meetings/2018/. Contributions in this and related areas of research are invited to contribute a special issue "*Advancing Earth Surface Representation via Enhanced Use of Earth Observations in Monitoring and Forecasting Applications*" in the journal Remote Sensing. Finally, the 3rd International Surface Working Group (ISWG-3) is planned for 9-11 July 2019, in Montréal Canada. An announcement with further details will be available in October of 2018.

Author
Dr. Ben Ruston, Ben.Ruston@nrlmry.navy.mil

2018 Colloquium Summary

The triennial Joint Center for Satellite Data Assimilation (JCSDA) Summer Colloquium was conducted July 22 - August 3, 2018, in Bozeman, Montana. The audience consisted of graduate students, early post-docs, and early career professionals whose work is moving them into satellite data assimilation. The fifteen (15) students who took part in the Bozeman Colloquium proved to be an exceptionally well-prepared and motivated group, and in fact, several of them recently have begun working or collaborating with the JCSDA or with one or

(continued on page 30)

another of the partner agencies or associated cooperative institutes.

The components for successful operational environmental modeling frequently are analogized as a three-legged stool requiring balanced contributions of observations, high-performance computing, and science as encapsulated in the development and improvement of the model and data assimilation systems. The strength of each of these legs depends on the availability of a talented and energetic workforce whose capabilities, collectively and individually, spans a broad set of science and technology disciplines. From the inception of the JCSDA, we have recognized that recruiting, developing, and nurturing that workforce is essential to our mission. The flagship of our efforts in this arena is the Summer Colloquium.

Following a formula refined over four (4) previous colloquia, the program consisted of four lectures daily presented in the morning and early afternoon. The lectures progressed from fundamentals including the formulation of the DA problem and general methodologies, consideration of computational constraints, the global observation system, and the preponderance of satellite data among those available to environmental modelers. Satellite orbits and sensors were treated in detail. The principles of radiative transfer and its application via the Community Radiative Transfer Model (CRTM) were introduced and microwave and infrared sounder radiance assimilation covered. Additional lectures covered other observation types and their assimilation for numerical weather prediction (NWP) models, including Atmospheric Motion Vector (AMV) winds, conventional observations, and Global Navigation Satellite System Radio Occultation (GNSSRO).

Subsequently, attention was given to calibration and validation of satellite observations, bias correction, analysis uncertainty, and estimation of data impacts in NWP systems, including the use of Observing System Simulation Experiments (OSSEs) for proposed sensors and missions. More specialized applications, such as aerosols and atmospheric composition, clouds and precipitation, mesoscale, tropical cyclone, land, and ocean, were addressed in turn, before coupled assimilation and development of the Joint Effort for Data assimilation Integration (JEDI) were taken up. The final lectures emphasized assimilation of new sensors, non-Gaussian applications, and the role of the JCSDA itself. The full agenda may be found on the JCSDA webpage.

To illustrate the lecture material, PC-based practical exercises were conducted every afternoon.

The formal proceedings each day concluded with two or three presentations by students on their recent, ongoing, or planned work. These provided a variety of benefits allowing the students to get research advice from the lecturers who typically were on hand for two-three days and opening the door for more extended conversations over breaks and meals. Bozeman provided an ideal environment to carry on after hour discussions with scenic views and opportunities to walk/hike in small groups

(continued on page 31)

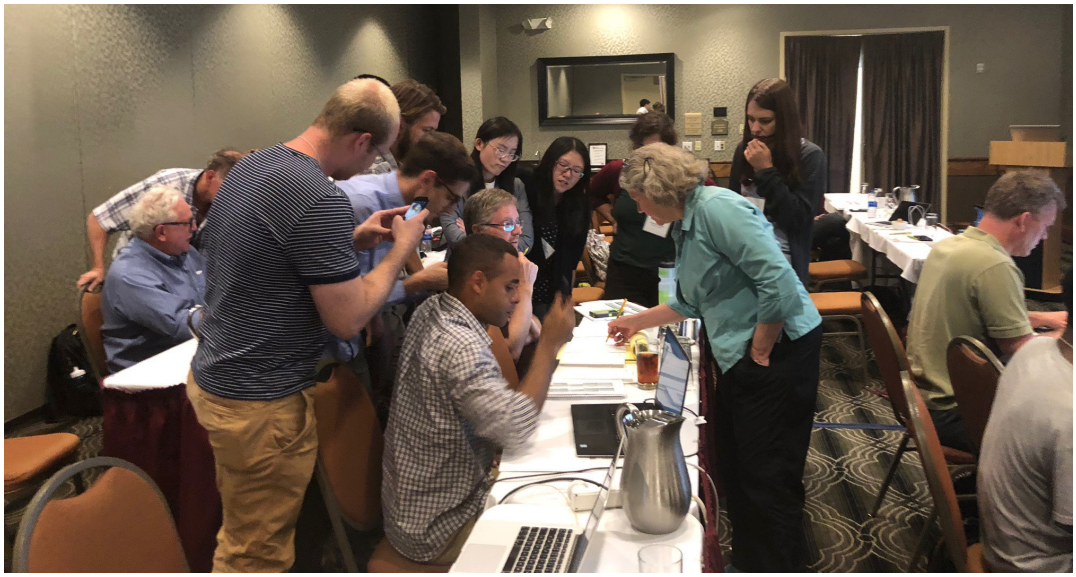

Students collaborating with one another on computer practical under guidance of Dr. Nancy Baker of the Naval Research Laboratory.)

on weekdays and to explore the local attractions more broadly on the weekend.

Thanks are due to National Oceanic and Atmospheric Administration (NOAA) National Environmental Satellite, Data, and Information Service (NESDIS) Center for Satellite Applications and Research (STAR) for supporting most of the students who took part and from all of the JCSDA partner agencies who sent lecturers. The program was organized by JCSDA Director, Tom Auligne, Nancy Baker and Jim Yoe of the JCSDA executive team, Steve Fletcher of Cooperative Institute for Research in the Atmosphere (CIRA) Colorado State University (CSU), and Daryl Kleist of NOAA/Environmental Modeling Center (EMC). Logistic support and arrangement for hotel, meeting facilities, and travel were provided through CIRA, particularly by Steve Fletcher and Holli Knudsen. Last but not least, Steve Fletcher served as de facto social secretary organizing numerous activities that built the commaradie of the group.

(continued on page 32)

PEOPLE

Introducing Dr. Daniel Holdaway

Dr. Daniel Holdaway joined the JCSDA in May 2018, as a member the Joint Effort for Data assimilation Integration (JEDI) development team. Daniel's initial responsibility will be to implement a JEDI-based data assimilation system for NCEP's FV3-GFS and NASA's GEOS atmospheric models on their native FV3 grids. Using the tangent linear and adjoint versions of FV3, developed by NASA's Global Modeling and Assimilation Office (GMAO), Daniel plans to implement a hybrid 4D-Var data assimilation system. He will also help implement a hybrid 4DEnVar system in conjunction with parallel work on a JEDI-based EnKF. In addition to the general model, interfacing this work will involve modeling background error covariance on the cube-sphere grid and interfacing to the Unified Forward Operator (UFO). Daniel also plans to implement the forecast sensitivity observation impacts (FSOI) tool within the JEDI framework, which involves the construction of the solver adjoints in the Object-Oriented Prediction System (OOPS). In the longer-term, Daniel looks forward to harnessing the flexibility of JEDI to address a number of interesting scientific problems, such as coupled data assimilation. Daniel will be located at NASA's Global Modeling and Assimilation Office (GMAO) in Greenbelt, MD.

Daniel undertook a PhD in mathematics at the University of Exeter in the UK. His studies focused on the interaction of the normal modes of the atmosphere when coupling dynamics and physics. Specifically, he was interested in how computational modes, present for certain grid staggering configurations, would behave in the presence of coupling.

Prior to joining the JCSDA, Daniel worked for NASA's GMAO for around seven years. During his time there, he worked on developing the adjoint of the GEOS model for use in the operational adjoint-based FSOI system and the GSI 4D-Var data assimilation system. He developed the adjoint of the FV3 dynamical core used in NASA's GOES and NCEP's FV3-GFS models. He also developed adjoint versions of the convection, cloud, radiation, turbulence, and GOCART dust physics. Daniel has addressed a number of interesting research questions using adjoint models, such as whether Saharan dust strengthens or weakens tropical cyclones, what caused the unique southern hemisphere sudden stratospheric warming, and why Hurricane Joaquin was so poorly forecast.

In his spare time, Daniel enjoys windsurfing, cycling, travelling, and playing soccer.

(continued on page 33)

EDITOR'S NOTE

Greetings!

Publishing a periodical makes one regard the passage of time with a measure of dismay. The deadlines for collecting, editing, and sending for layout articles and other contributions for the upcoming issue populate the calendar almost as soon as the previous issue is distributed. But as the inputs are collected, it's always gratifying to recognize how much work is underway and how much is being accomplished in the JCSDA community. This edition is no exception.

Several recent newsletters have focused on preparation for evaluating and exploiting observations from a single satellite mission or sensor. In contrast, you will find in this issue a diverse selection of science articles. For example, S. Albert and Z. Toth have contributed one describing the use of sky cameras to validate and augment satellite-/ radar-based cloud assimilation, while T.C. Chen has provided a piece about the efficient data selection method for NWP using ensemble forecast sensitivity to observations. Not least, D. Kleist has written a summary of plans for data assimilation for the Next Generation Global Prediction System (NGGPS-FV3GFS) at NOAA. It's fair to say that there's something for almost everyone.

Summer tends to be a busy time for our community and for many of us being busy has entailed traveling. The Joint Workshop of the International Surface Working Group (ISWG) and the Land Surface Analysis Satellite Application Facility (LSA-SAF) was in Lisbon, Portugal, at the end of June. A detailed summary of the proceedings, outcomes, and anticipated next steps can be found in this issue courtesy of Ben Ruston of the Naval Research Laboratory and two international colleagues, Giancarlo Balsamo and Isabel Franco Trigo.

The JCSDA was well represented at the Workshop on Sensitivity Analysis and Data Assimilation in Meteorology and Oceanography (more commonly known as the "Adjoint Workshop") in Aveiro, Portugal, in early July, with Tom Auligne, Director of the JCSDA, and Nancy Baker, Ron Gelaro, and Daryl Kleist of the Executive Team all taking part. While a range of topics was covered, prominent themes of several talks included model errors in data assimilation, accounting for correlated observation error, atmosphere-ocean coupled assimilation, and various approaches for assessing observation impact. As is the tradition at the Adjoint Workshop, most presentations were punctuated by numerous questions and vigorous discussion. On a more personal note, the attendees formally recognized and thanked Ron Errico for serving as lead organizer of all eleven Adjoint Workshops to date, beginning in 1992. Finally, the JCSDA Summer Colloquium for graduate students and early post-docs was held July 22 - August 3, in Bozeman, MT, and a summary of this event is provided too.

(continued on page 34)

For a community that is so dispersed by organization and geography, the introduction of new staff via the newsletter is a necessity. In this issue, you have the opportunity to meet Daniel Holdaway, who has joined the JCSDA core staff, working at Goddard Space Flight Center in Greenbelt, MD. On the other hand, we recently bade farewell to a long-standing member of the JCSDA Executive Team, as Associate Director, John Derber of the NCEP's Environmental Modeling Center, retired from federal service in July. We are fortunate that Dr. Daryl Kleist has been selected to serve as NCEP's Associate Director for the JCSDA in the future. Finally, on the Management Oversight Board Colonel, Jeffrey Jarry of the USAF has moved on to a new assignment. He will be replaced by a familiar figure, Dr. Mike Farrar. We thank those who are leaving our company for their service to the JCSDA, and we welcome those who are coming aboard.

I hope you find this newsletter informative and inspiring - Jim

SCIENCE CALENDAR

UPCOMING EVENTS

MEETINGS AND EVENTS SPONSORED BY JCSDA

DATE	LOCATION	WEBSITE	TITLE
November 12–16, 2018	College Park, MD, USA		JEDI Academy
January 6–10, 2019	Phoenix, AZ, USA	https://annual.ametsoc.org/index.cfm/2019/programs/conferences-and-symposia/seventh-ams-symposium-on-the-joint-center-for-satellite-data-assimilation/	7th AMS Symposium on the Joint Center for Satellite Data Assimilation

MEETINGS OF INTEREST

DATE	LOCATION	WEBSITE	TITLE
November 5–9, 2018	Seoul, Korea	http://www.isac.cnr.it/~ipwg/	IPWG
December 10–14, 2018	Washington, D.C., USA	https://fallmeeting.agu.org/2018/	AGU fall meeting
January 6–10, 2019	Phoenix, AZ, USA	https://annual.ametsoc.org/2019/	99th AMS Annual Meeting

CAREER OPPORTUNITIES

Opportunities in support of JCSDA may also be found at http://www.jcsda.noaa.gov/careers.php as they become available.